Targeted Foxe1 Overexpression in Mouse Thyroid Causes the Development of Multinodular Goiter But Does Not Promote Carcinogenesis

Alyaksandr Nikitski, Vladimir Saenko, Mika Shimamura, Masahiro Nakashima, Michiko Matsuse, Keiji Suzuki, Tatiana Rogounovitch, Tetiana Bogdanova, Nobuyuki Shibusawa, Masanobu Yamada, Yuji Nagayama, Shunichi Yamashita, and Norisato Mitsutake

Departments of Radiation Medical Sciences (A.N., M.M., K.S., S.Y., N.M.), Radiation Molecular Epidemiology (V.S., S.Y.), Molecular Medicine (M.S., Y.N.), Global Health, Medicine and Welfare (T.R.), and Department of Tumor and Diagnostic Pathology (M.N.), Atomic Bomb Disease Institute, Nagasaki University; Nagasaki University Graduate School of Biomedical Sciences (A.N.); and Nagasaki University Research Centre for Genomic Instability and Carcinogenesis (N.M.), Nagasaki 852-8523, Japan; Laboratory of Morphology of Endocrine System (T.B.), State Institution V.P. Komisarenko Institute of Endocrinology and Metabolism of Academy of Medical Sciences of Ukraine, Kyiv 254114, Ukraine; and Department of Medicine and Molecular Science (N.S., M.Y.), Gunma University Graduate School of Medicine, Maebashi, Gunma 371-8511, Japan

Recent genome-wide association studies have identified several single nucleotide polymorphisms in the forkhead box E1 gene (*FOXE1*) locus, which are strongly associated with the risk for thyroid cancer. In addition, our recent work has demonstrated FOXE1 overexpression in papillary thyroid carcinomas. To assess possible contribution of Foxe1 to thyroid carcinogenesis, transgenic mice overexpressing Foxe1 in their thyroids under thyroglobulin promoter (*Tg-Foxe1*) were generated. Additionally, *Tg-Foxe1* mice were exposed to x-rays at the age of 5 weeks or crossed with *Pten*$^{+/-}$ mice to examine the combined effect of Foxe1 overexpression with radiation or activated phosphatidylinositol-3-kinase/Akt pathway, respectively. In 5- to 8-week-old *Tg-Foxe1* mice, severe hypothyroidism was observed, and mouse thyroids exhibited hypoplasia of the parenchyma. Adult 48-week-old mice were almost recovered from hypothyroidism, their thyroids were enlarged, and featured colloid microcysts and multiple benign nodules of macrofollicular-papilloid growth pattern, but no malignancy was found. Exposure of transgenic mice to 1 or 8 Gy of x-rays and *Pten* haploinsufficiency promoted hyperplastic nodule formation also without carcinogenic effect. These results indicate that Foxe1 overexpression is not directly involved in the development of thyroid cancer and that proper Foxe1 dosage is essential for achieving normal structure and function of the thyroid. **(*Endocrinology* 157: 2182–2195, 2016)**

FOXE1 is a thyroid-specific forkhead transcription factor crucial for craniopharyngeal embryogenesis and for the maintenance of differentiated state of thyroid. Germline loss-of-function forkhead box E1 gene (*FOXE1*) mutations in humans are the basis for the rare autosomal-recessive Bamforth-Lazarus syndrome characterized by cleft palate, spiky hair, choanal atresia, bifid epiglottis, and congenital hypothyroidism (CH) due to thyroid dysgenesis (1). Foxe1 deficiency in mice also leads to developmental abnormalities such as thyroid ectopy or loss of thyroid follicular cell (TFC) progenitors. Interestingly, the initiation of thyroid primordium formation at early stages of embryogenesis and functional differentiation of the TFC precursors are not impaired in Foxe1-null mice (2).

ISSN Print 0013-7227 ISSN Online 1945-7170
Printed in USA

Received December 18, 2015. Accepted March 10, 2016.
First Published Online March 16, 2016

Abbreviations: BAT, brown adipose tissue; CH, congenital hypothyroidism; *Dio1*, type I deiodinase; FOXE1, forkhead box protein E1; FT_4, free T_4; IHC, immunohistochemistry; *Pax8*, paired box gene 8; PI3K-Akt, phosphatidylinositol-3-kinase-Akt; PTC, papillary thyroid carcinoma; PTEN, phosphatase and tensin homolog; qRT-PCR, quantitative real-time RT-PCR; RT, room temperature; SV-40, simian virus 40; TFC, thyroid follicular cell; TTF, thyroid transcription factor; WT, wild type.

In functionally differentiated human TFC, FOXE1 regulates several thyroid-specific genes such as *TG*, *TPO*, *NIS*, and *DUOX2* (3, 4), acting as a classical pioneer transcription factor (5, 6). FOXE1 is a useful marker of differentiated state of normal or neoplastic thyroid tissues, and its expression correlates with differentiation level of thyroid cancer cells. Previous studies showed that FOXE1 expression is significantly down-regulated in poorly differentiated thyroid carcinoma and is absent in anaplastic thyroid cancer (7, 8). On the other hand, our recent work has demonstrated FOXE1 overexpression and cytoplasmic translocation in human papillary thyroid carcinoma (PTC) (9). FOXE1 expression is not only elevated in PTC but also correlates with some clinicopathological features such as extracapsular invasion, tumor stage, and lymph node metastasis (10). Moreover, recent genome-wide and target gene association studies have identified 2 single-nucleotide polymorphisms, rs965513 located 60 kb upstream of *FOXE1* and rs1867277 in the 5′ untranslated region of the same gene, which confer risk for thyroid cancer (11, 12). These single-nucleotide polymorphisms may be involved in transcriptional regulation of *FOXE1*. For instance, the risk allele of rs1867277 (A) enhances the activation of *FOXE1* promoter in Hela cells through the recruitment of upstream stimulatory transcription factors (13). Nevertheless, the precise role of FOXE1 in thyroid tumorigenesis is not fully understood so far.

To assess possible contribution of Foxe1 to thyroid carcinogenesis, we generated transgenic mice overexpressing Foxe1 under thyroglobulin promoter (*Tg-Foxe1*). Additionally, *Tg-Foxe1* mice were exposed to x-rays at the age of 5 weeks or crossed with $Pten^{+/-}$ mice to address the combined effect of Foxe1 overexpression with radiation or activated phosphatidylinositol-3-kinase-Akt (PI3K-Akt) pathway, respectively. Surprisingly, we found that *Tg-Foxe1* mice developed thyroid hypoplasia and overt hypothyroidism shortly after birth but at older age had multinodular goiter. Congenital hypothyroidism (CH) is observed in 1:2000 to 1:4000 of neonates (14, 15). The vast majority (up to 85%) of primary CH cases are caused by thyroid dysgenesis associated with loss-of-function mutations in *TSHR*, *PAX8*, *NKX2–1*, *FOXE1*, and *NKX2–5*, whereas dyshormonogenesis accounts for 10%–15% of cases due to mutations in *SLC5A5*, *TPO*, *DUOX2*, *DUOXA2*, *SLC26A4*, *TG*, and *IYD/DEHAL1* (16, 17). It should be noted that follicular (18–22) and PTC (23–26) may arise from dyshormonogenetic goiter. No data on FOXE1 overexpression in CH or its effect on either human or murine thyroid is available, and comprehensive understanding of CH with subsequent goiter or thyroid carcinogenesis is impeded by the lack of adequate animal models.

Here, we introduce the first mouse model of thyroid-specific overexpression of Foxe1 and provide a detailed histopathological characterization of Foxe1-associated hypothyroidism followed by the development of multinodular goiter. The combined effect of Foxe1 overexpression with x-ray irradiation or activated PI3K-Akt pathway is also presented.

Materials and Methods

Mice

A mouse model of targeted expression of Foxe1 driven by the bovine thyroglobulin promoter was generated. Fragment of the bovine thyroglobulin promoter (2045 bp), the murine *Foxe1* gene (1116 bp) and the simian virus 40 (SV-40) polyadenylation signal (228 bp) were cloned into the pBlue-script-II SK+ vector (Stratagene). For transgenesis, purified construct DNA was microinjected into zygotes and transferred into pseudopregnant C57BL/6J females at the UNITECH facility (Chiba, Japan). Transgene integration into the genome of founders was confirmed by Southern blotting. Two independent lines were established. Founder mice were mated with wild-type (WT) C57BL/6J partners, and the progeny was screened for the presence of transgene by PCR as described below. Heterozygous *Pten*-knockout mice (B6.129-*Pten*<tm1Rps>, hereafter designated as $Pten^{+/-}$ mice) were obtained from National Cancer Institute at Frederick. Double transgenic mice were obtained by cross-mating of *Tg-Foxe1* mice with $Pten^{+/-}$ mice.

Mice were bred in a specific pathogen-free facility and fed with a standardized regular diet. Animal care and all experimental procedures were performed in accordance with the Guidelines for Animal Experimentation of Nagasaki University with the approval of the Institutional Animal Care and Use Committee.

PCR genotyping

Genotyping was performed at the age of 4 weeks by PCR using tail-extracted DNA (REDExtract-N-Amp Tissue PCR kit; Sigma) or amnion-derived DNA for embryos. The primers used to detect the *Tg-Foxe1* transgene were: 5′-CTACAGCCTCCACAAGATTTTCA-3′ and 5′-TGAGTTTGGACAAACCACAACTA-3′ yielding a 1552-bp PCR product. The primers for $Pten^{+/-}$ mice were: P012 (5′-TTGCACAGTATCCTTTTGAAG-3′) and P013 (5′-GTCTCTGGTCCTTACTTCC-3′) yielding a 240-bp product for WT *Pten*; and P012 and P014 (5′-ACGAGACTAGTGAGACGTGC-3′) yielding a 320-bp product for *Pten*.

X-ray irradiation

WT and *Tg-Foxe1* littermates were exposed to 1 or 8 Gy of x-rays at the age of 5 weeks. Mice were anesthetized by ip injection of Nembutal (sodium pentobarbital) into the lower left quadrant of abdomen at a dose of 40 mg/kg and immobilized. Unshielded front neck area was exposed to x-rays at a dose rate of 0.5531 Gy/min using a Toshiba ISOVOLT TITAN 320.

Animal groups and tissue and serum sampling

In the present study, mice were divided into 4 main groups according to the genetic background: C57BL/6J WT mice, *Tg-Foxe1*, *Pten*$^{+/-}$, and double transgenic *Tg-Foxe1/Pten*$^{+/-}$. Not exposed to x-ray WT and *Tg-Foxe1* mice were subdivided into 4 age groups: 5–8 and 24–48 weeks; mice exposed to x-ray were killed at the age of 8, 24, and 48 weeks. *Pten*$^{+/-}$ and *Tg-Foxe1/Pten*$^{+/-}$ mice were examined at the age of 5–8 and 24 weeks.

At the indicated time points, mice were anesthetized by ip injection of Nembutal at the dose of 50 mg/kg. Blood was collected by cardiac puncture, and the animals were euthanized by cervical dislocation. Thyroid lobes were dissected and weighted. One lobe was snap-frozen in liquid nitrogen and stored at −80°C until use, and the other was put in 10% neutral-buffered formalin. After 24 hours of fixation in formalin at 4°C, tissue samples were rinsed in water and embedded into paraffin. Five-micrometer-thick serial sections were prepared for further hematoxylin-eosin or immunohistochemical staining. For cryosectioning, fresh tissue samples were washed in ice-cold PBS and frozen in Tissue-Tek O.C.T. compound (Sakura Finetek). Sections were taken in a cryostat Leica CM3050 S (Leica Biosystems).

Brown adipose tissue (BAT) staining

Cryosections were fixed in 10% formalin for 15 minutes at 4°C. After intensive washing in distilled water, slides were incubated in propylene glycol 2 × 5 minutes and stained with 150nM solution of Sudan Black B in propylene glycol for 7 minutes with agitation. After washing for 3 minutes in 85% propylene glycol and rinsing in distilled water, sections were counterstained with Nuclear Fast Red (Sigma) for 5 minutes and mounted with aqueous mounting media.

Immunohistochemistry (IHC)

Formalin-fixed paraffin-embedded 4-μm serial sections were deparaffinized and subjected to antigen retrieval in a microwave in Tris-EDTA buffer (pH 9.0), at 95°C for 25 minutes (for Foxe1 antigen unmasking) or in citrate buffer (pH 6.0), at 95°C for 25 minutes (for Ttf-1, thyroglobulin, calcitonin, and Ki-67 antigens unmasking). Blocking reagent (Dako) was applied at room temperature (RT) for 1 hour. After blocking, the sections were incubated with primary antibodies diluted in Antibody Diluent (Dako) solution: rabbit anti-thyroid transcription factor-1 (anti-TTF1;1:750; Biopat), rabbit anti-thyroid transcription factor-2 (anti-TTF2; 1:750; Biopat), rabbit antithyroglobulin (1:1000; Dako), rat anti-Ki-67 (1:100; Dako), rabbit anti-phosphatase and tensin homolog (1:400; Abcam), and anticalcitonin (prediluted; Dako) overnight at 4°C. After washing, horseradish peroxidase-conjugated secondary antibodies antirabbit (1:100; Dako) or antirat (1:100; Dako) were applied for 1 hour at RT. Detailed information about antibodies used in this study is presented in Supplemental Table 1. Visualization was performed with DAB Enhanced Liquid Substrate System tetrahydrocloride (Sigma). Nuclei were counterstained with hematoxylin.

The intensity score of nuclear Foxe1 staining was categorized as negative (0), weak (1), mild (2), or strong (3). The proportion score was determined as a percentage of positively stained nuclei of thyroid epithelial cells within the intensity category. The total Foxe1 IHC-score was calculated as a sum of products of staining intensity scores and corresponding proportion scores. Ki-67 labeling index was calculated as a percentage of positively stained nuclei of thyroid epithelial cells. At least 1000 thyroid epithelial cells were counted in 5 random fields at ×400 magnification for evaluation of the Foxe1 IHC-score and Ki-67 labeling index.

Dual-labeled immunofluorescence analysis

Formalin-fixed paraffin-embedded 4-μm sections were deparaffinized and subjected to antigen retrieval in a microwave in Tris-EDTA buffer (pH 9.0), at 95°C for 20 minutes. Sections were blocked for 1 hour in 5% BSA in PBS and incubated with primary antibodies diluted in 5% skim milk in tris-buffered saline containing 0.05% Tween-20: rabbit anti-TTF2 (1:250; Biopat) and rat anti-Ki-67 (1:50; Dako) overnight at 4°C. Sections were then incubated with 4′, 6-diamidino-2-phenolindole (1:1000; Dojindo) and secondary antibodies diluted in 5% skim milk in tris-buffered saline containing 0.05% Tween-20: anti-rabbit Alexa Fluor 546 and antirat Alexa Fluor 647 (1:1000; Invitrogen) for 1 hour at RT. Stained slides were imaged using a BZ-9000 microscope (Keyence) and were recorded with a BZ-II analysis application (Keyence). Exposition time for 450-, 546-, and 647-nm signals were optimized to obtain the widest dynamic range of recorded fluorescence intensity.

Quantitative real-time RT-PCR (qRT-PCR)

Total RNA was extracted from homogenized fresh-frozen thyroid tissues with ISOGEN reagent (Nippon Gene). A total of 200 ng of total RNA were transcribed with ReverTra Ace qPCR RT Master Mix with gDNA Remover (Toyobo). Quantitative PCR was carried out in a Thermal Cycler Dice Real-Time System (Takara Bio, Inc) using SYBR Premix Ex Taq II reagent (Takara Bio, Inc). The profile of thermal cycle was as follows: 95°C for 2 minutes, 40 cycles of 95°C for 5 seconds, and 60°C for 30 seconds, followed by dissociation curve analysis for all primer pairs. The average of the relative quantity of replicates was calculated with Q-Gene software (27) using β-actin (*Actb*) or paired box gene 8 (*Pax8*) data for normalization. Sequences of the primers are listed in Supplemental Table 2.

Serum free T_4 (FT_4), FT_3, and TSH measurement

FT_4 and FT_3 were measured using standard laboratory assay (SRL, Inc). Mouse serum TSH was measured using in-house RIA as described previously (28).

Statistical analysis

Statistical comparison of categorical variables was performed using the 3 × 2 or 4 × 2 extensions of Fisher's exact test (http://in-silico.net/tools/statistics/fisher_exact_test/2x3). Continuous data were analyzed by applying nonparametrical Mann-Whitney *U* test for comparison of 2 groups or Kruskal-Wallis test for multiple group comparisons as appropriate. Analysis was performed with IBM SPSS Statistics version 21 and GraphPad 4.1 Prism (GraphPad Software) software packages. All *P* values were 2-sided and considered significant if less than 0.05.

Results

Generation of *Tg-Foxe1* mice

For thyroid-specific overexpression of Foxe1, a 3.4-kb genetic construct combining the bovine thyroglobulin

promoter, the murine *Foxe1*, and the simian virus 40 (SV-40) polyadenylation signal was created (Figure 1A). Two independent founder lines bearing 12 (line A) and 2 (line B) copies of the transgene were established. Both lines developed similar thyroid phenotype within 48 weeks of life span (Supplemental Figure 1A). Transgenic *Foxe1* expression was verified by qRT-PCR with transgene-specific primers (Supplemental Figure 1B). The line A bearing a greater number of transgene copies was chosen for the detailed investigation.

qRT-PCR assessment of transgenic *Foxe1* expression demonstrated its age-dependent decline (Figure 1B). Total *Foxe1* expression (ie, endogenous and transgenic *Foxe1* combined) did not change with age in WT mice but was decreasing in *Tg-Foxe1* animals (Figure 1C). By the age of 48 weeks, no difference in total *Foxe1* expression was observed between transgenic and WT animals. The decrease in total *Foxe1* expression in *Tg-Foxe1* mice with age is thus likely to be fully attributed to the decline in the expression of the *Foxe1* transgene.

Foxe1 overexpression in the thyroids of *Tg-Foxe1* mice was confirmed by IHC (Figure 1D). The proportion of cells showing the highest score (3, strong) of immunoreactivity to Foxe1 remained significantly higher in *Tg-Foxe1* mice compared with WT at all age groups (Figure 1E), but the drastic difference at 5–8 weeks declined at 24–48 weeks. Similar observations were made for the total Foxe1 IHC score (Figure 1F). The results of IHC corresponded well with qRT-PCR data.

Systemic characterization of the *Tg-Foxe1* mice

No obvious differences between newborn *Tg-Foxe1* mice and their WT siblings were observed. However, the signs of growth retardation became apparent 2–3 weeks after birth. The *Tg-Foxe1* mice exhibited cretinous body habitus (Figure 2A) and significantly lower body weight in both males and females until the age of 8 weeks (Figure 2B). The thyroid weights of 5- and 8-week-old *Tg-Foxe1* mice were comparable with those of WT mice but became significantly greater at 24 and 48 weeks (Figure 2C). The thyroid weight to body weight ratio was significantly higher in *Tg-Foxe1* than in WT mice at 8, 24, and 48 weeks but not at 5 weeks (Figure 2D). Gross anatomy of transgenic animals was normal except thyroid. As representatively shown for the 48-week-old mice (Figure 2E), *Tg-Foxe1* animals had enlarged thyroids with irregular surface and visible nodules.

Taking into consideration the essential role of Foxe1 in thyroid primordium migration and TFC precursors survival, mouse embryos were examined histologically. Thyroid bud formation and migration of TFC precursors towards the front neck area was not altered. The thyroid reached its conventional position at embryonic day 14.5. The appearance of isolated TFC highly positive for Foxe1 in embryonic day 14.5 transgenic mice (Supplemental Figure 2A) coincided with the onset of thyroglobulin expression (29). The ultimobranchial bodies were successfully enclosed by thyroid tissue. As a result, widely disseminated calcitonin-positive cells were detected in the thyroids of postnatal transgenic animals (Supplemental Figure 2B).

Tg-Foxe1 mice developed hypothyroidism

Because of the pronounced growth retardation in transgenic mice, serum TSH, FT_4, and FT_3 were measured. TSH levels were significantly elevated and FT_4 diminished in 5- and 8-week-old *Tg-Foxe1* mice (Figure 3). Despite that there was no difference in TSH levels between *Tg-Foxe1* and WT mice in 24- to 48-week-old animals, serum FT_4 was gradually increased but not fully recovered. We also measured serum FT_3 in *Tg-Foxe1* and WT mice, and surprisingly, they were not different in all age group (Figure 3). We therefore examined the expression of type I deiodinase (*Dio1*) and *Dio2* in the extracted thyroid lobes. Both *Dio1* and *Dio2* expression in *Tg-Foxe1* mice were robustly up-regulated in young animals and then declined but still remained higher than in WT mice even at the older age (Supplemental Figure 3), which may be the reason for imbalance between FT_4 and FT_3.

We also measured transcriptional levels of thyroid-specific genes *Slc5a5* (sodium/iodide symporter, *Nis*), thyroid peroxidase (*Tpo*), dual oxidase 2 (*Duox2*), and *Slc26a4* (pendrin, *Pds*), which could be regulated by Foxe1 and are involved in thyroid hormone biosynthesis. Compared with WT mice, all except *Duox2* were age dependently up-regulated, presumably due to corresponding Foxe1 overexpression, but none was suppressed (Supplemental Figure 3). Therefore, hypothyroidism in young *Tg-Foxe1* mice was not caused by the disruption of thyroid hormone biosynthesis and was mainly due to thyroid hypoplasia (see histological description below). On the whole, our observations indicate that *Tg-Foxe1* mice exhibited severe hypothyroidism in young age and a gradual recovery until 48 weeks.

Histological features of the thyroid in young (5- to 8-wk-old) mice

At the age of 5–8 weeks, thyroids of WT animals showed predominantly normomicrofollicular structure without pathological abnormalities. In contrast, thyroids of *Tg-Foxe1* mice displayed the abnormal irregular architecture with dominant micronormofollicular, minor macrofollicular, solid, and papilloid areas (Figure 4, A and B). Thyroid epithelium in the papilloid areas showed some

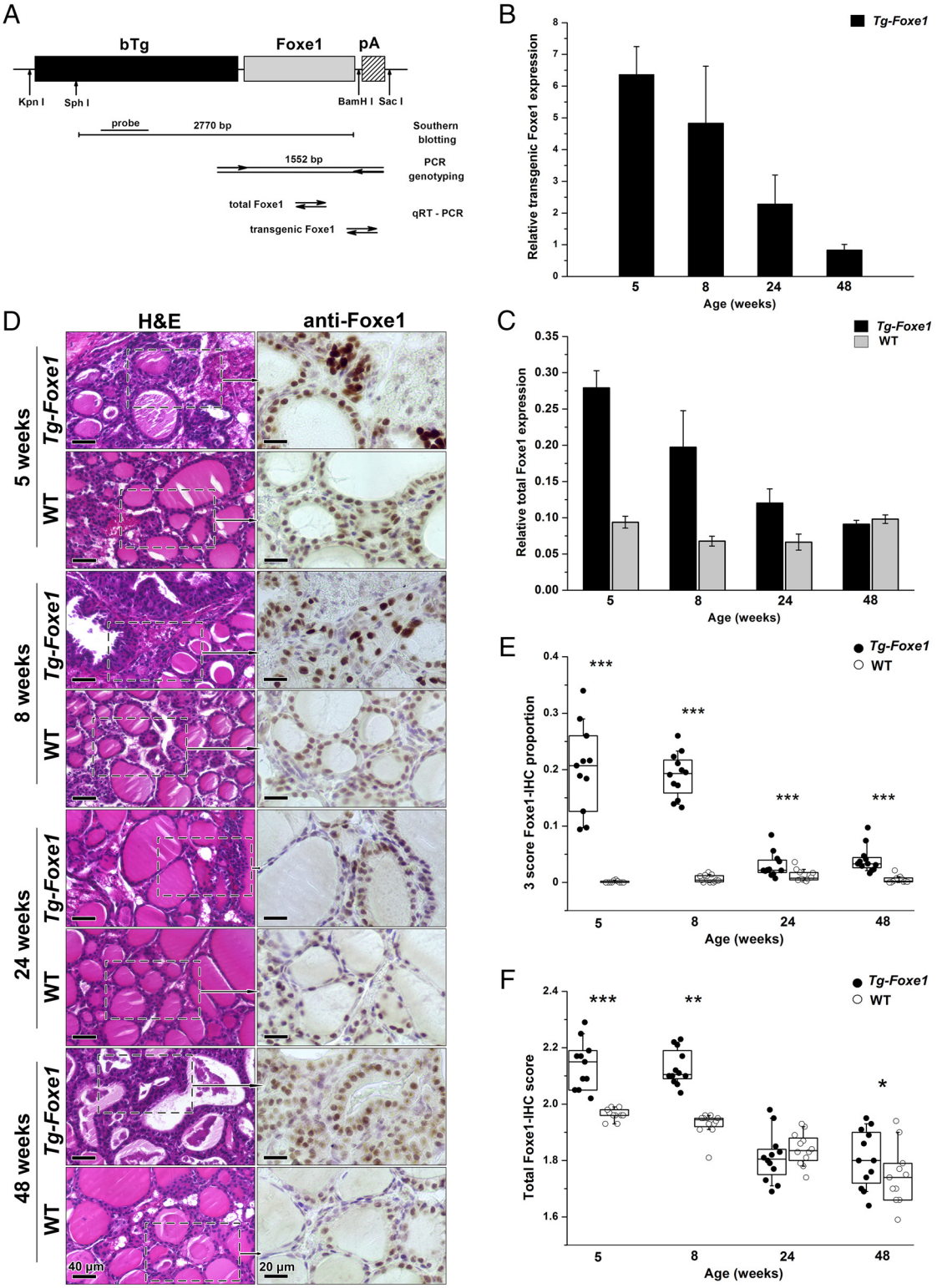

Figure 1. Generation and analysis of *Tg-Foxe1* mice. A, The genetic construct used to generate the *Tg-Foxe1* mice. The bovine thyroglobulin promoter (bTg, 2045 bp), murine *Foxe1* gene (*Foxe1*, 1116 bp), and the SV-40 polyadenylation signal (pA, 228 bp) are indicated by the rectangles. For Southern blotting, the 2770-bp *SphI*/*Bam*HI restriction fragment was hybridized with a probe located in the bTg area. For PCR screening of the *Foxe1* transgene, primers were designed to amplify the 1552-bp region spanning the bTg and pA sequences. B, Relative cDNA levels of transgenic *Foxe1* in the thyroid of *Tg-Foxe1* line A determined by qRT-PCR and normalized for *Pax8* expression. For qRT-PCR assessment of transgenic *Foxe1* expression, primers located in the 3′ end of *Foxe1* and in pA sequences were used. Data are presented as a mean ± SE of triplicates averaged for 8 mice for each group. C, Relative cDNA levels of total *Foxe1* in the thyroids of WT and *Tg-Foxe1* line A determined by qRT-PCR and normalized for *Pax8* expression. For qRT-PCR assessment of *Foxe1* expression, primers located in the coding region of *Foxe1* were used. Data are presented as a mean ± SE of triplicates averaged for 8 mice for each group. D, Representative images of thyroid histology and Foxe

oxyphilic changes. The number of thyroid follicles in the young transgenic animals was decreased in comparison with the control littermates; normal parenchyma was abundantly substituted by BAT (Figure 4A) as confirmed by staining of thyroid cryosections with Sudan Black B and qRT-PCR for *Ucp1* (Supplemental Figure 4, A and B). In some animals, BAT occupied more than 40% of the thyroid volume (Supplemental Figure 4C). In *Tg-Foxe1* mice, thyroid follicles were predominantly filled with pale colloid; some follicles contained heterogeneous, foamed or depleted colloid (Figure 4B, b).

Thyroid follicles in WT mice were predominantly lined by a single uniform layer of cuboidal epithelium and a small fraction of flattened epithelial cells at the periphery of the gland. Besides conventional epithelium, thyroids of *Tg-Foxe1* mice featured tall cuboidal and columnar follicular cells (Figure 4B, b). Thyrocytes of young Foxe1 overexpressing mice also displayed prominent nuclear pleomorphism and hyperchromatosis, especially in solid clusters; giant hyperchromatic/bizarre nuclei were also revealed.

Functional differentiation of TFCs was confirmed by IHC for thyroglobulin, Ttf-1, and Foxe1 (Figure 5A). Interestingly, some thyrocytes in transgenic animals showed stronger cytoplasmic thyroglobulin staining than in control mice. The intensity and proportion of Ttf-1 staining was similar between *Tg-Foxe1* and WT littermates. The intensity of Foxe1 immunoreactivity was heterogeneous in thyrocytes in both transgenic and WT mice. Nevertheless, the total Foxe1 IHC-score was significantly higher in 5- to 8-week-old transgenic mice in comparison with WT animals (see also Figure 1F). Small immature follicles contained thyrocytes with the highest intensity of Foxe1 staining were commonly seen (Figure 5A, arrow in the Foxe1 panel), whereas in mature follicles and areas of focal hyperplasia, such cells were less frequent.

In transgenic mice, tall cuboidal and columnar thyrocytes had eosinophilic cytoplasm likely due to a high level of TSH stimulation. Concordantly, a proliferative index estimated by Ki-67 IHC (Figure 5B) was significantly higher as compared with that in WT animals both in 5- to 8-week-old males and females (Figure 6A). Histologically, the high level of follicular cell proliferation activity was represented by numerous papilloid structures inside follicular lumens and initial signs of hyperplastic nodule formation (as was demonstrated in Figure 4, A and B). Interestingly, Ki-67-positive follicular cells had moderate to low levels of Foxe1 (Figure 5C), strongly suggesting that cells overexpressing Foxe1 were unlikely to be involved in the active proliferation upon TSH stimulation.

Histological features of the thyroid in mature/adult (24- to 48-wk-old) mice

The thyroids of WT mice at 24–48 weeks displayed normomacrofollicular structure with normal age-associated histopathological changes. In transgenic mice, from the age of 24 weeks, hyperplastic areas of diffuse macrofollicular structure and hyperplastic micronodules were observed. The number of cells with nuclear pleomorphism and hyperchromatosis were drastically decreased in adult *Tg-Foxe1* mice in comparison with 5- to 8-week-old ones. Marked accumulation of the colloid resulted in dilatation of follicles and formation of colloid microcysts. (Figure 4, C and D). Gradual decrease of BAT content was also noted (Supplemental Figure 4C).

At 24–48 weeks, follicular epithelium of WT mice was predominantly cuboid and, to a less extent, flattened. In *Tg-Foxe1* mice, macrofollicular thyroid structures contained somewhat flattened cuboid or fully flattened cells (Figure 4D, a). At the age of 48 weeks, well-formed hyperplastic, predominantly macrofollicular-papilloid micronodules in transgenic mice were seen (Figure 4D). Enlarged follicles contained papilloid projections of cuboid or columnar eosinophilic cells with pleomorphic nuclei (Figure 4D, b). Hyperplastic papilloid micronodules in *Tg-Foxe1* mice did not show any specific features of PTC such as capsular/lymphovascular invasion or nuclear grooves, pseudoinclusions and optical clearing. Small hyperplastic follicles protruding into the lumen of larger follicles, so called Sanderson's pollsters, were also found.

At the age of 24–48 weeks, transgenic mice, both males and females, showed lower Ki-67 labeling indexes compared with 5- to 8-week-old mice. Nevertheless, it remained significantly higher as compared with that in WT animals (Figure 6). Thus, by the age of 48 weeks *Tg-Foxe1* mice did not develop thyroid cancer, but the gland was affected by a diffuse macrofollicular hyperplastic process with multiple macronormopapilloid hyperplastic micronodules and colloid microcysts.

Effect of x-ray exposure

Irradiation of thyroids of WT mice with 1 or 8 Gy of x-rays at the age of 5 weeks resulted in prominently flattened follicular epithelium and dilatation of the follicular lumen at the age of 48 weeks in comparison with nonexposed mice (Figure 7A). Exposure of *Tg-Foxe1* mice sig-

Figure 1 (Continued). 1 immunoreactivity in WT and *Tg-Foxe1* mice of different age. H&E and IHC for Foxe1. E and F, The proportion of cells with the highest intensity score (3, strong) in Foxe1 IHC. F, The total Foxe1 IHC score. In E and F, the boxes include 50% of the values; lines inside the boxes represent median values; whiskers indicate the 10%–90% range; *, $P < .01$; **, $P < .001$; ***, $P < .0001$.

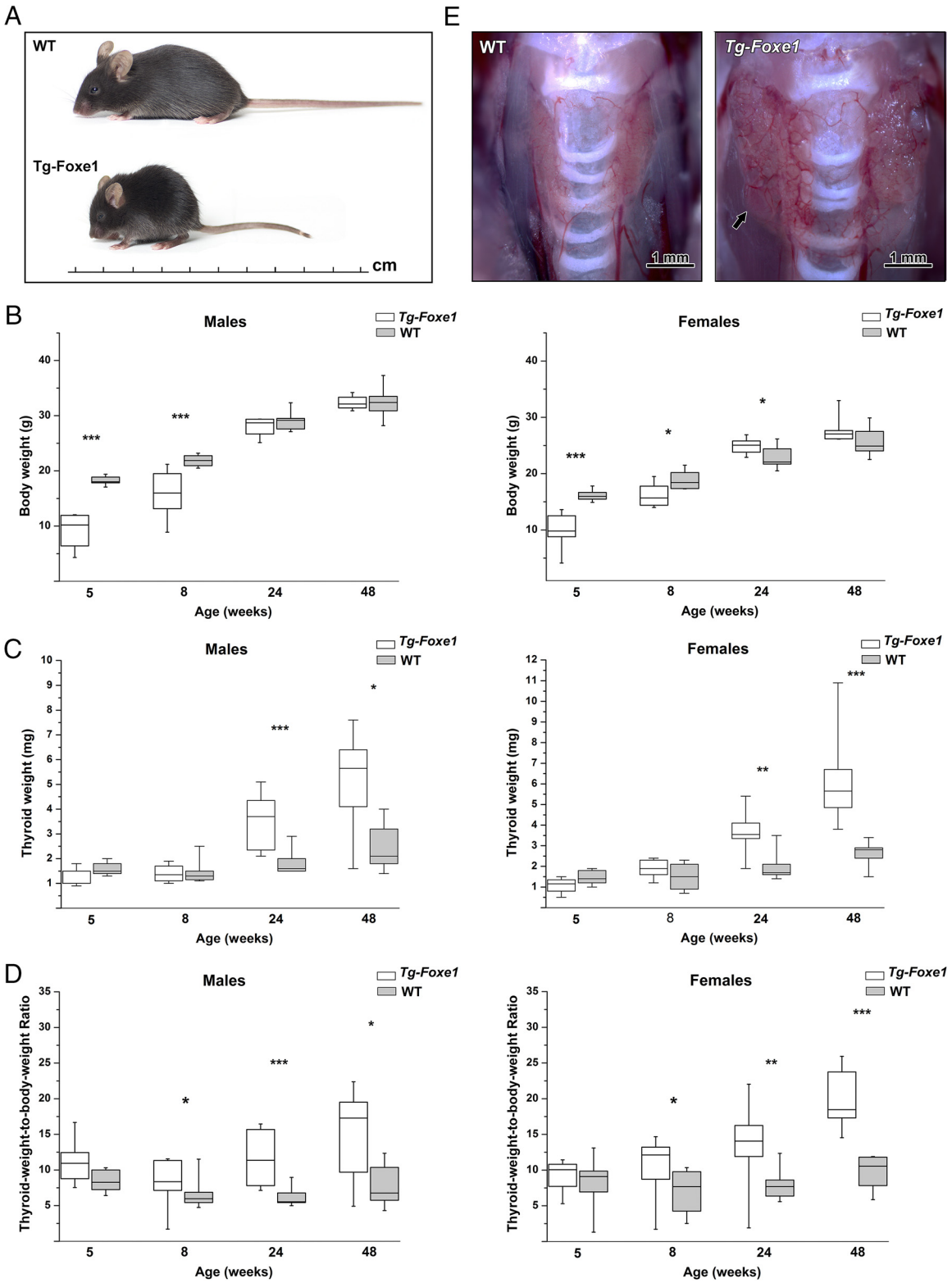

Figure 2. Systemic characterization of *Tg-Foxe1* mice. A, Body habitus of representative female WT and *Tg-Foxe1* mice at the age of 5 weeks. Body weight (males n = 7–24 mice/group, females n = 8–38 mice/group) (B), thyroid weight (males n = 5–16 mice/group, females n = 8–38 mice/group) (C), and thyroid to body weight ratio (males n = 5–16 mice/group, females n = 8–38 mice/group) (D) in WT and *Tg-Foxe1* animals of different age. Boxes include 50% of the values; lines inside the boxes represent median values; whiskers indicate the 10%–90% range; *, $P < .01$; **, $P < .001$; ***, $P < .0001$. E, Gross anatomy of WT and *Tg-Foxe1* mouse thyroids at the age of 48 weeks. Arrow points at the irregular surface of the thyroid.

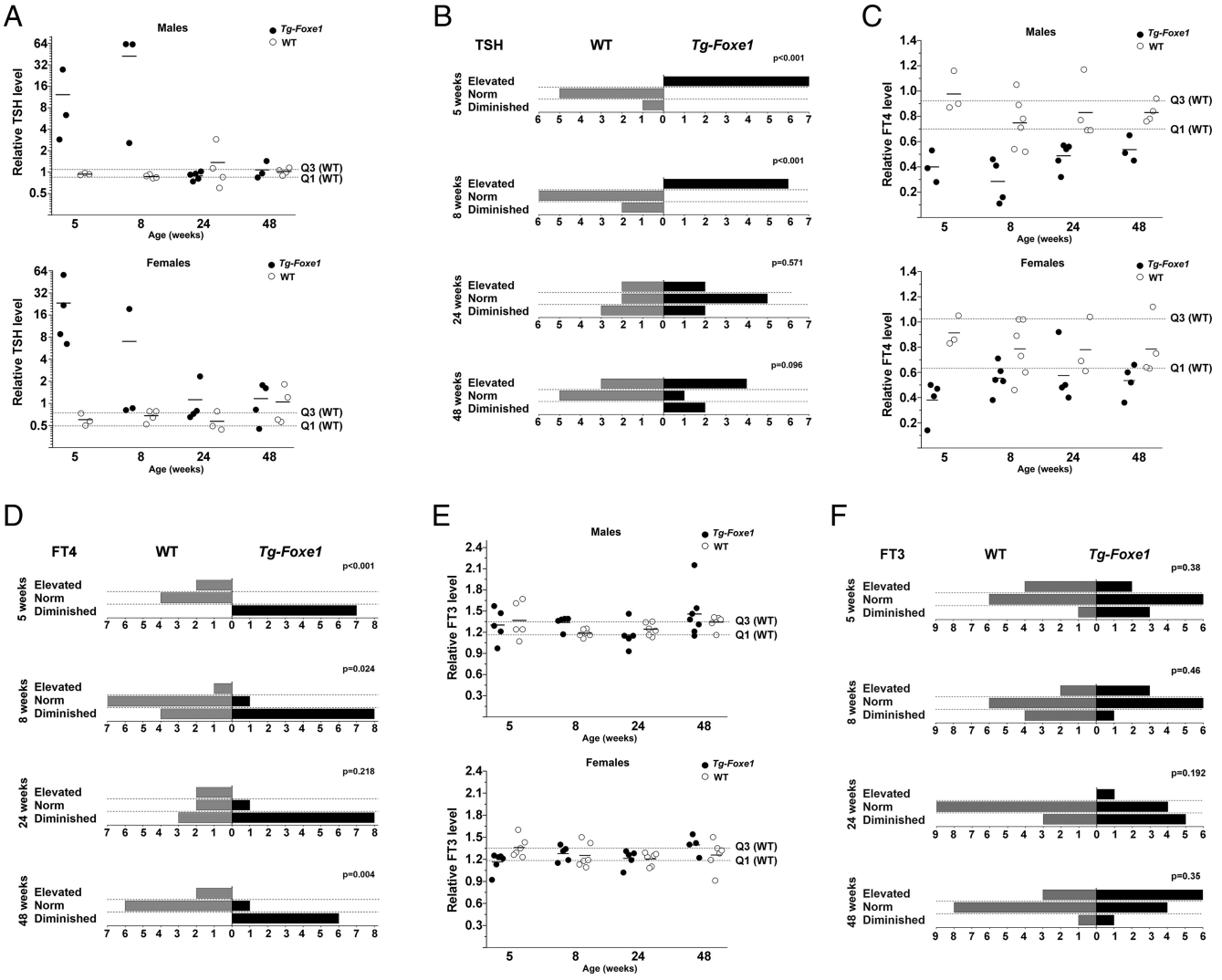

Figure 3. The hypothyroid status of *Tg-Foxe1* mice. A, C, and E, Relative TSH (A), FT_4 (C), and FT_3 (E) levels in WT and *Tg-Foxe1* mice of different age. The median value is represented by the solid line. Horizontal dashed lines represent the first (Q1) and the third quartile (Q3) of the relative TSH or FT_4 values in WT mice estimated for each sex separately (see below). TSH (B), FT_4 (D), and FT_3 (F) level category in WT (n = 6–11 mice/group) and *Tg-Foxe1* (n = 6–9 mice/group) animals of different age combined for both sexes (see below). Because of limitations in the in-house produced reagent availability and small sample volumes, statistical analysis of raw TSH, FT_4, and FT_3 concentrations in separate subgroups of male and female animals was impeded. We therefore determined the normal ranges of relative sex-specific TSH and FT_4 levels as intervals between Q1and Q3 calculated from the integrated data across all age groups of WT mice (distributions between which did not differ significantly, $P > .05$, Kruskal-Wallis test). The defined normal ranges of relative TSH level in WT mice were 0.85–1.06 ng/mL (n = 15) and 0.52–0.78 ng/mL (n = 14) for males and females, respectively; 0.70–0.92 ng/dL (n = 17) and 0.63–1.02 ng/dL (n = 16) for FT_4; and 1.16–1.38 pg/mL (n = 23) and 1.18–1.35 pg/mL (n = 24) for FT_3. Then each raw value was categorized as diminished (<Q1), normal (Q1–Q3), or elevated (>Q3) for either TSH, FT_4 or FT_3. This approach allowed merging data for 2 sexes to increase statistical power. Differences between WT (n = 6–11 mice/group) and *Tg-Foxe1* (n = 6–11 mice/group) animals were evaluated using the 3 × 2 Fisher's exact test extension.

nificantly promoted hyperplastic micronodule formation (Figure 7B). After exposure to 1 Gy, well-formed hyperplastic micronodules were found from 8 weeks of age and from 24 weeks after 8 Gy. Despite the delay in micronodule formation (as compared with 1-Gy exposure), a significantly higher frequency of micronodules was observed in the latter group at 48 weeks of age ($P < .01$). Histopathological features of thyroid micronodules in exposed *Tg-Foxe1* animals were similar to those in unexposed transgenic mice of the same age. Thus, exposure of Foxe1-overexpressing animals to ionizing radiation stimulated the formation of hyperplastic nodules in a dose-related manner without carcinogenic effect.

Double transgenic *Tg-Foxe1/Pten*$^{+/-}$ mice

Double transgenic *Tg-Foxe1/Pten*$^{+/-}$ animals developed severe hypothyroidism at the age of 5 weeks similarly to *Tg-Foxe1* mice. CH was characterized by significant growth retardation, significantly elevated serum TSH, and diminished FT_4 (data not shown). Thyroid follicular epi-

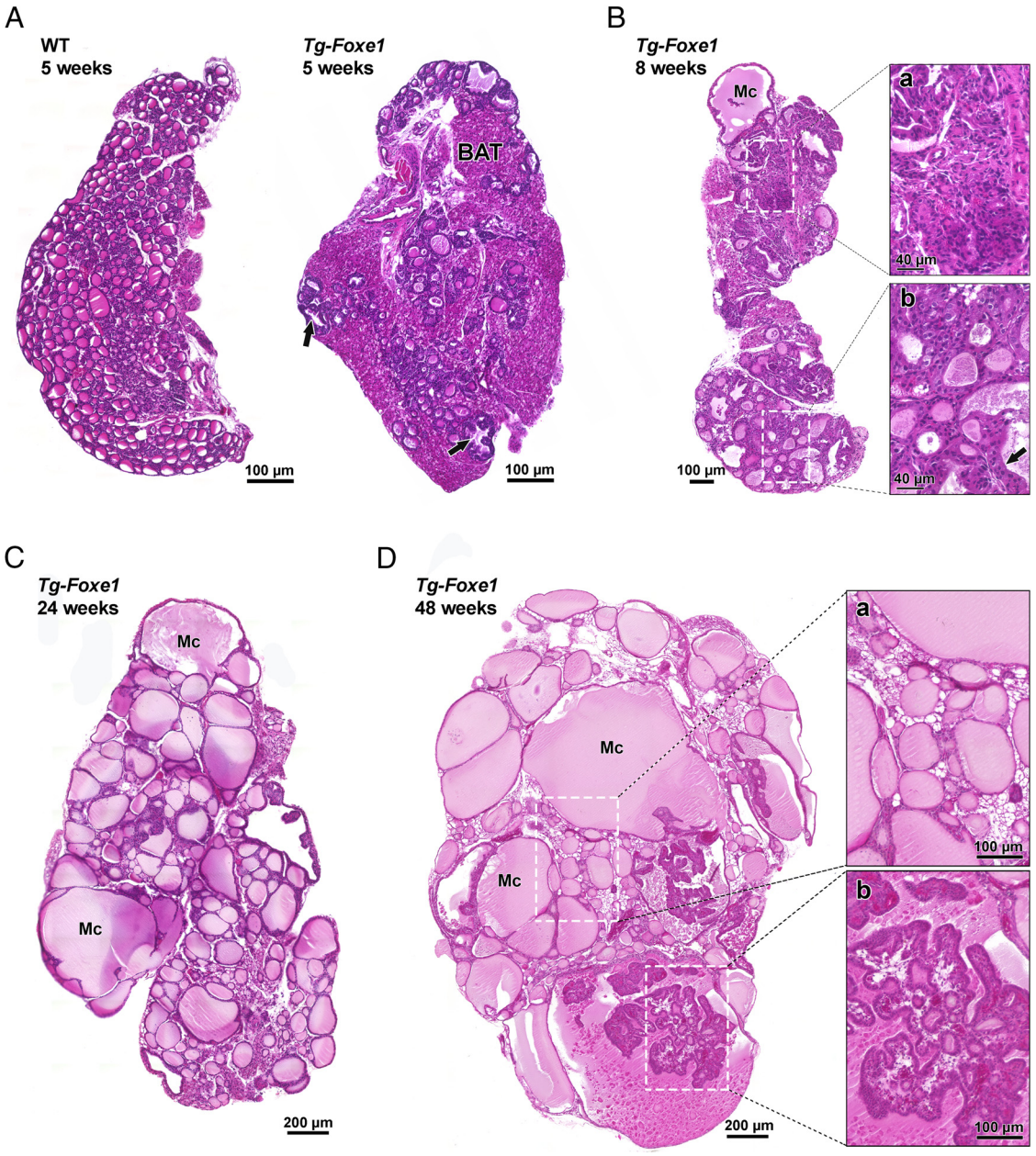

Figure 4. Histopathology of the *Tg-Foxe1* thyroid at different age. A, Representative microphotographs of *Tg-Foxe1* and WT mice thyroids at the age of 5 weeks, H&E staining. BAT denotes BAT, arrows point at foci of hyperplastic micronodules. B, The representative image of 8-week-old *Tg-Foxe1* thyroid with a colloid microcyst (Mc) and featuring (a) abnormal solid/papilloid structures, and (b) colloid heterogeneity and columnar follicular epithelium (arrow). C, The representative image of 24-week-old *Tg-Foxe1* thyroid. D, The representative image of 48-week-old *Tg-Foxe1* thyroid; (a) area with flattened thyroid epithelium and (b) a nodule with papilloid structures.

thelium was profoundly substituted by BAT. Colloid in normo-, micro-, and macrofollicles was heterogeneous: pale, depleted, foamed, and sometimes with mucinous content. Cellular areas showing pleomorphism of follicular cells with nuclear enlargement and hyperchromasia were observed.

Activation of the follicular epithelium in 5- to 8-week-old *Tg-Foxe1/Pten*$^{+/-}$ mice was observed: cuboidal thyrocytes had increased eosinophilic cytoplasm with small clear vacuoles. Hyperplastic changes such as papilloid projections into the follicular lumen, nuclear crowding, and foci of columnar cells were more frequent in 5- to 8-week-old double transgenic mice in comparison with age-matched *Tg-Foxe1* and *Pten*$^{+/-}$ mice. The proliferation rate of thyroid epithelial cells in *Tg-Foxe1/Pten*$^{+/-}$ mice was significantly higher in comparison with *Pten*$^{+/-}$ animals at 5 and 8 weeks of age (Figure 6). Immunohistochemical staining showed that there was no loss of the remaining *Pten* allele in any age group (Supplemental Figure 5). Ki-67 labeling indexes did not differ significantly between *Tg-Foxe1/*

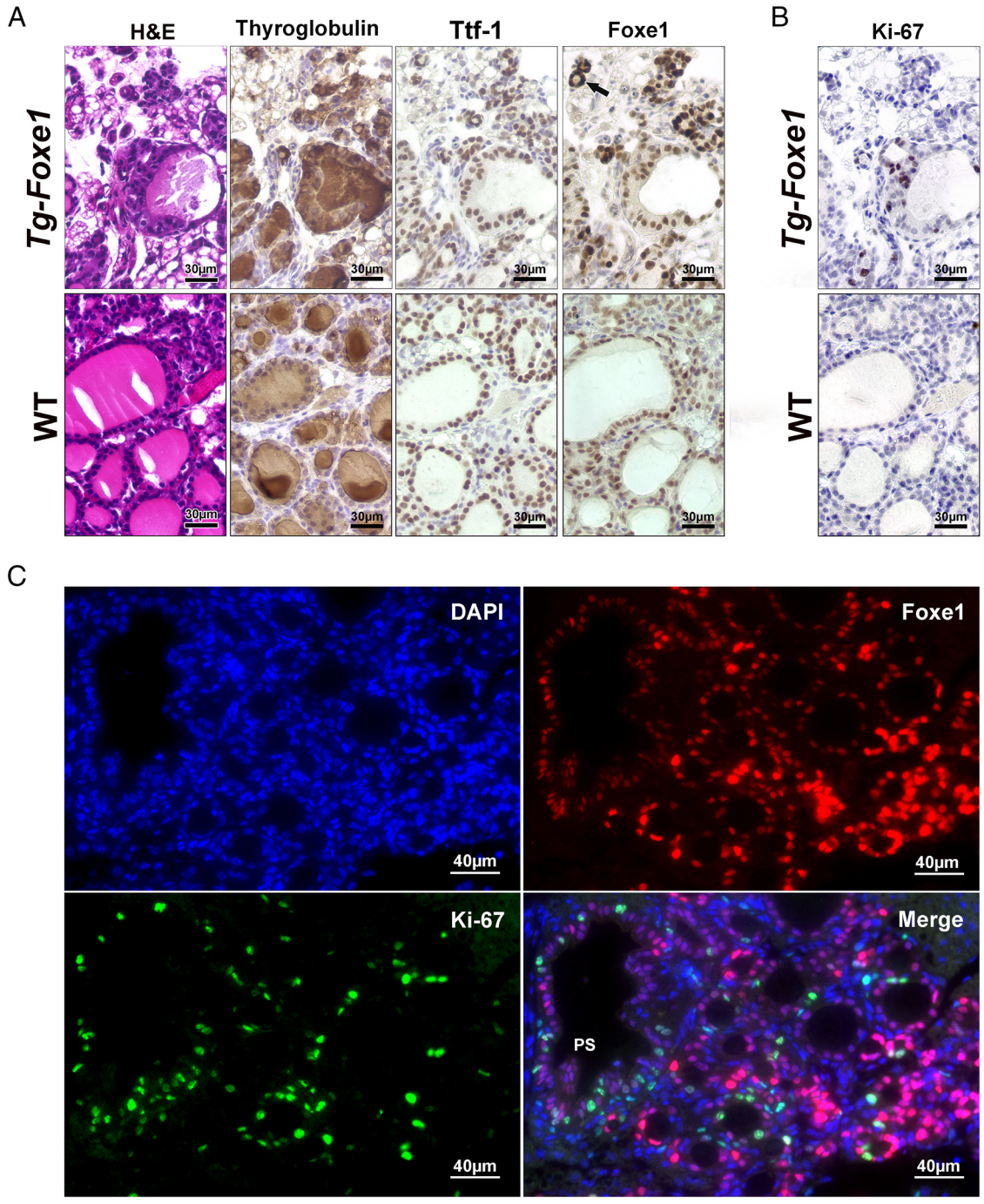

Figure 5. Functional differentiation and proliferative status of thyroid cells in young *Tg-Foxe1* and *WT* mice. A, H&E and IHC for thyroglobulin, Ttf-1, and Foxe1, serial sections. The arrow in the Foxe1 panel indicates immature follicle with high Foxe1 level. B, IHC for Ki-67. C, Double immunofluorescent staining for Ki-67 (green) and Foxe1 (red). Nuclei were counterstained with 4′, 6-diamidino-2-phenolindole (DAPI). PS, papillary structures.

Pten$^{+/-}$ and *Tg-Foxe1* mice in all age groups (Figure 6), indicating that heterozygous *Pten* deletion added a minor effect on the proliferative phenotype of *Tg-Foxe1* mice thyroids. On the other hand, the labeling indexes in *Tg-Foxe1/Pten*$^{+/-}$ and *Tg-Foxe1* mice were significantly higher than in age-matched WT animals (Figure 6).

In contrast to *Tg-Foxe1* and *Pten*$^{+/-}$ mice, double transgenic animals developed multiple hyperplastic thyroid micronodules from the age of 8 weeks (Figure 7, C and D). The frequency of micronodules in *Tg-Foxe1/Pten*$^{+/-}$ mice was significantly higher in comparison with *Pten*$^{+/-}$ animals. Note that *Pten*$^{+/-}$ mice had predominantly adenomatous nodules with normomicrofollicular-solid or normofollicular-solid structure, prominent oxyphilic changes of follicular cells and areas of nuclear pleomorphism. Micronodules in double transgenic mice

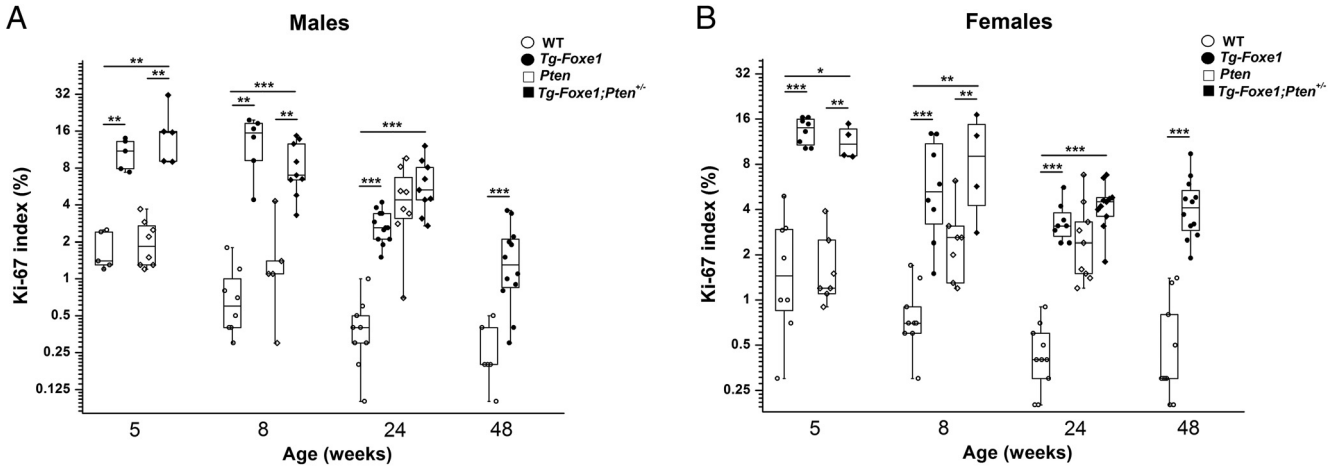

Figure 6. Ki-67 labeling index in the thyroids of mice of different age. A, WT (n = 5–9 mice/group), *Tg-Foxe1* (n = 5–16 mice/group), $Pten^{+/-}$ (n = 5–8 mice/group) and *Tg-Foxe1*/$Pten^{+/-}$ (n = 5–9 mice/group) males. B, WT (n = 8–10 mice/group), *Tg-Foxe1* (n = 8–12 mice/group), $Pten^{+/-}$ (n = 7–9 mice/group) and *Tg-Foxe1*/$Pten^{+/-}$ (n = 4–11 mice/group) females. Boxes include 50% of the values; lines inside the boxes represent median values; whiskers indicate the 10%–90% range; *, $P < .05$; **, $P < .01$; ***, $P < .001$.

showed mixed features of hyperplastic nodules found in *Tg-Foxe1* mice and adenomatous nodules of $Pten^{+/-}$ animals (Figure 7C). Thus, Foxe1 overexpression in thyroids of $Pten^{+/-}$ mice caused acceleration of hyperplastic processes, showing features of both $Pten^{+/-}$ and *Tg-Foxe1* phenotypes, but no cancerous nodules were seen.

Discussion

To evaluate the role of high level of Foxe1 as a possible etiological factor in thyroid carcinogenesis, transgenic mice overexpressing *Foxe1* under the thyroglobulin promoter were generated. The transgenic animals were viable and showed no apparent gross developmental abnormalities. However, in the postnatal period, *Tg-Foxe1* mice at the age 5–8 weeks displayed CH manifesting as significant growth retardation, diminished level of FT_4 and elevated TSH. In those mice, normal follicular organization in the thyroid gland was compromised, and thyroid parenchyma was replaced with BAT to a large extent.

Under the TSH stimulation, tall cuboidal and columnar thyrocytes with augmented eosinophilic cytoplasm appeared in the thyroids of transgenic mice. TSH-induced enhancement of thyroid hormone synthesis was accompanied by the activation of endocytosis in thyrocytes seen as colloid depletion in some follicles. High TSH levels also switched on the growth of thyroid parenchyma. The thyroids of 5-week-old transgenic mice showed a high (>10%) Ki-67 labeling index. It is worth noting, however, that follicular cells overexpressing Foxe1 were unlikely to be the primary responders to TSH stimulation. Several facts concordantly support this notion: 1) in the areas of evident proliferation, most cells displayed moderate levels of Foxe1 on IHC or immunofluorescence; 2) the proportion of cells with strong Foxe1 staining intensity was declining with the increase of thyroid weight; 3) small immature follicles highly immunoreactive for Foxe1 persisted in the thyroids of 5- to 8-week-old *Tg-Foxe1* mice; and 4) no Ki-67 signals were seen in the cells overexpressing Foxe1. It is likely that Foxe1 overexpression may prevent the proliferative cellular reaction on TSH stimulation. Under this scenario, thyroid parenchyma regeneration and hyperplastic changes seen in older mice would be achieved through the propagation of epithelial cells with lower Foxe1 level. The inability of cells with high Foxe1 levels to proliferate is also consistent with and may explain thyroid hypoplasia observed during the first month of postnatal life of *Tg-Foxe1* mice. Molecular mechanisms of interference between the proliferative signals and Foxe1 overexpression as well as age-dependent down-regulation of transgene expression require further investigation.

TSH-induced activation and proliferation of follicular cells led to the gradual increase of FT_4 level. However, surprisingly, the FT_3 level in the *Tg-Foxe1* mice was not different from WT mice in all age groups. This may be due to the increased level of *Dio1* and *Dio2* in the thyroids of the transgenic animals. *Dio1* and *Dio2* were highly up-regulated in the 5- to 8-week-old *Tg-Foxe1* mice, in which BAT occupied a large part of thyroid tissue. It should be mentioned that TSH receptors are expressed in BAT cells and TSH stimulates *Dio2* expression in these cells (30).

Exposure of *Tg-Foxe1* mice thyroids to 1 or 8 Gy of x-rays at the age of 5 weeks accelerated hyperplastic nodule formation in a dose-dependent manner. The

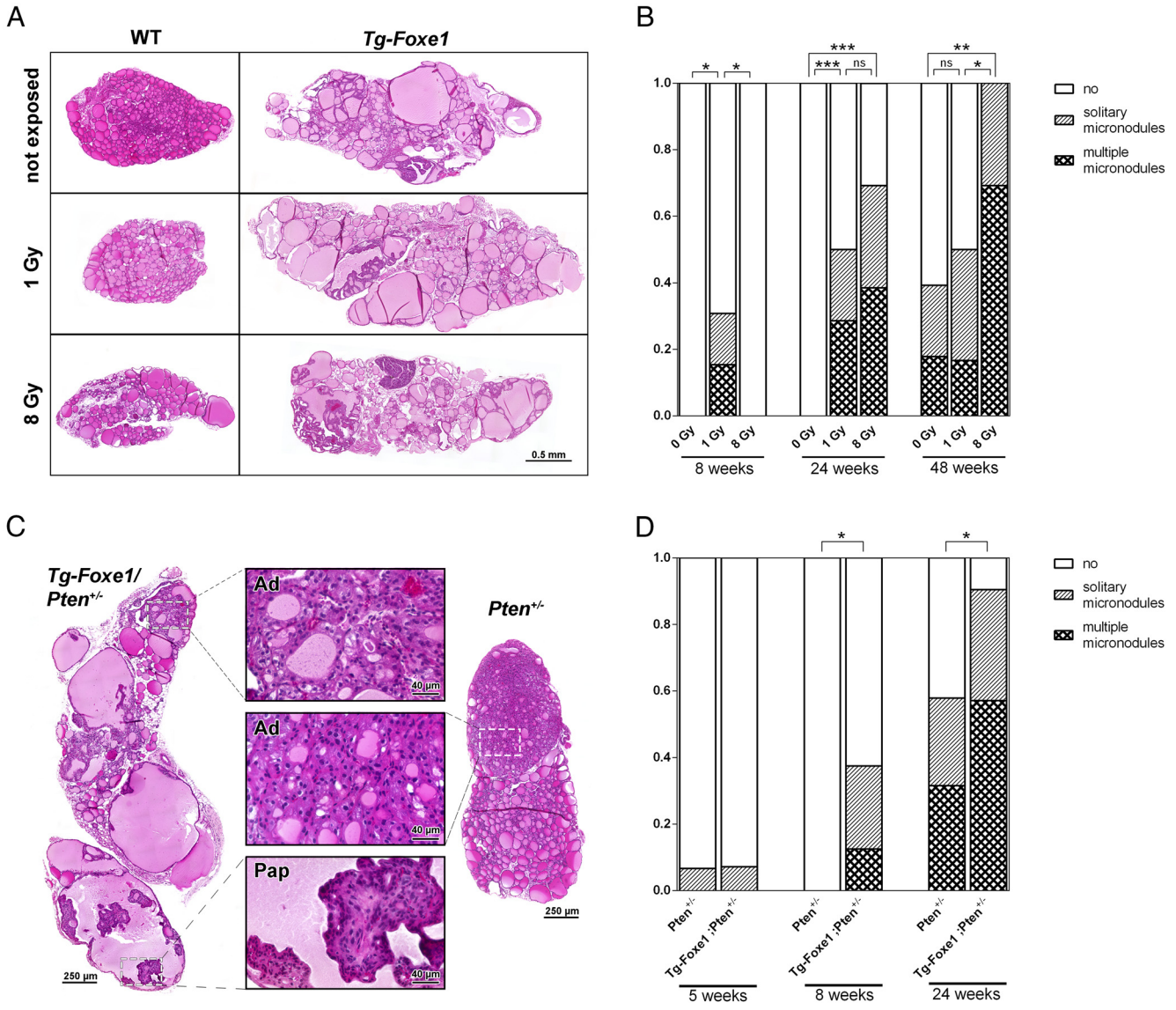

Figure 7. Combination effect of Foxe1 overexpression with x-ray irradiation or activated PI3K-Akt signaling pathway. A, Representative microphotographs showing x-ray-associated histopathological changes in WT and *Tg-Foxe1* mice thyroids at the age of 48 weeks, H&E staining. Scale bar, 0.5 mm, applies to all microphotographs. B, Frequencies of micronodule finding in thyroids of *Tg-Foxe1* mice of different age by x-ray dose. Differences between unexposed (n = 14–28 mice/group), and exposed to 1 Gy (n = 12–14 mice/group) or 8 Gy (n = 13–14 mice/group) of x-rays, mice were evaluated using the 3 × 2 Fisher's exact test extension: *, $P < .01$; **, $P < .001$; ***, $P < .0001$; ns, not significant. C, Representative images of histopathological features of thyroids in 24-week-old *Tg-Foxe1/Pten*$^{+/-}$ and *Pten*$^{+/-}$ mice, H&E staining. Hyperplastic areas with adenomatous (Ad) and papillary (Pap) structures. D, Frequencies of micronodules in thyroids of *Tg-Foxe1/Pten*$^{+/-}$ (n = 14–21 mice/group) and *Pten*$^{+/-}$ (n = 15–17 mice/group) mice of different age; *, $P < .01$.

changes were observed from 8–24 weeks of age, whereas irradiated WT mice did not develop any thyroid lesions. We speculate that high TSH may promote metaplastic changes in the thyroid follicular epithelium exposed to x-ray irradiation. A similar effect of TSH could be proposed with regard to Foxe1 overexpression combined with the activated PI3K-Akt pathway. We found that hypothyroid 5-week-old *Tg-Foxe1/Pten*$^{+/-}$ mice exhibited a remarkable increase in the thyrocyte proliferation rate as compared with age-matched *Pten*$^{+/-}$ mice. Moreover, double transgenic mice displayed an accelerated formation of hyperplastic and adenomatous nodules detectable from the age of 8 weeks, whose development was not due to the loss of the remaining *Pten* allele. More detailed investigation is needed to establish exact pathogenetic and molecular basis of these hyperplastic and neoplastic processes.

The model described in our study has some limitations. The overexpression of Foxe1 caused hypothyroidism, thus corresponding TSH elevation in young mice, and the transgene expression was then declined with age. This created a complicated situation, which made it difficult to

assess the effect of Foxe1 overexpression only (ie, without the hormone imbalance) on thyroid tumorigenesis. On the other hand, all transgenic mice displayed thyroid-related phenotype, and therefore the model may be useful for in vivo studies of the mechanisms of TSH-dependent proliferation of the thyrocytes or BAT cells under the condition of CH, and of pathogenesis of multinodular goiter.

In summary, our mouse model of thyroid-specific overexpression of Foxe1 allowed us to make several important observations. By the age of 5 weeks, transgenic mice displayed thyroid hypoplasia accompanied by the extensive replacement of thyroid parenchyma with BAT and the development of overt hypothyroidism. Likely due to the prolonged TSH stimulation at young age, the reactive proliferation of TFC took place and resulted in the nearly full compensation of hypothyroidism by the age of 24 weeks and the development of hyperplastic changes representative of multinodular goiter. No direct evidence of thyroid carcinogenesis due to Foxe1 overexpression during the course of 48 week-long observation was found either in *Tg-Foxe1* mice, *Tg-Foxe1* mice exposed to 1–8 Gy of x-rays or in 24-week-old *Tg-Foxe1/Pten*$^{+/-}$ mice. We conclude that proper Foxe1 dosage is essential for thyroid development and functioning, and excessive Foxe1 in the thyroid does not induce carcinogenesis in our model.

Acknowledgments

Address all correspondence and requests for reprints to: Norisato Mitsutake, MD, PhD, Department of Radiation Medical Sciences, Atomic Bomb Disease Institute, Nagasaki University, 1-12-4 Sakamoto, Nagasaki 852-8523, Japan. E-mail: mitsu@nagasaki-u.ac.jp.

This work was supported in part by Grants-in-Aid for Scientific Research 26293142 (to N.M.) and 26293222 (to S.Y.) from the Japan Society for the Promotion of Science.

Disclosure Summary: The authors have nothing to disclose.

References

1. **Bamforth JS, Hughes IA, Lazarus JH, Weaver CM, Harper PS.** Congenital hypothyroidism, spiky hair, and cleft palate. *J Med Genet*. 1989;26:49–51.
2. **De Felice M, Ovitt C, Biffali E, et al.** A mouse model for hereditary thyroid dysgenesis and cleft palate. *Nat Genet*. 1998;19:395–398.
3. **Sinclair AJ, Lonigro R, Civitareale D, Ghibelli L, Di Lauro R.** The tissue-specific expression of the thyroglobulin gene requires interaction between thyroid-specific and ubiquitous factors. *Eur J Biochem*. 1990;193:311–318.
4. **Fernandez LP, Lopez-Marquez A, Martinez AM, Gomez-Lopez G, Santisteban P.** New insights into FoxE1 functions: identification of direct FoxE1 targets in thyroid cells. *PLoS One*. 2013;8:e62849.
5. **Cuesta I, Zaret KS, Santisteban P.** The forkhead factor FoxE1 binds to the thyroperoxidase promoter during thyroid cell differentiation and modifies compacted chromatin structure. *Mol Cell Biol*. 2007;27:7302–7314.
6. **Zaret KS, Carroll JS.** Pioneer transcription factors: establishing competence for gene expression. *Genes Dev*. 2011;25:2227–2241.
7. **Nonaka D, Tang Y, Chiriboga L, Rivera M, Ghossein R.** Diagnostic utility of thyroid transcription factors Pax8 and TTF-2 (FoxE1) in thyroid epithelial neoplasms. *Mod Pathol*. 2008;21:192–200.
8. **Sequeira MJ, Morgan JM, Fuhrer D, Wheeler MH, Jasani B, Ludgate M.** Thyroid transcription factor-2 gene expression in benign and malignant thyroid lesions. *Thyroid*. 2001;11:995–1001.
9. **Bychkov A, Saenko V, Nakashima M, et al.** Patterns of FOXE1 expression in papillary thyroid carcinoma by immunohistochemistry. *Thyroid*. 2013;23:817–828.
10. **Fan Y, Ding Z, Yang Z, et al.** Expression and clinical significance of FOXE1 in papillary thyroid carcinoma. *Mol Med Rep*. 2013;8:123–127.
11. **Gudmundsson J, Sulem P, Gudbjartsson DF, et al.** Common variants on 9q22.33 and 14q13.3 predispose to thyroid cancer in European populations. *Nat Genet*. 2009;41:460–464.
12. **Takahashi M, Saenko VA, Rogounovitch TI, et al.** The FOXE1 locus is a major genetic determinant for radiation-related thyroid carcinoma in Chernobyl. *Hum Mol Genet*. 2010;19:2516–2523.
13. **Landa I, Ruiz-Llorente S, Montero-Conde C, et al.** The variant rs1867277 in FOXE1 gene confers thyroid cancer susceptibility through the recruitment of USF1/USF2 transcription factors. *PLoS Genet*. 2009;5:e1000637.
14. **Toublanc JE.** Comparison of epidemiological data on congenital hypothyroidism in Europe with those of other parts in the world. *Horm Res*. 1992;38:230–235.
15. **Harris KB, Pass KA.** Increase in congenital hypothyroidism in New York State and in the United States. *Mol Genet Metab*. 2007;91:268–277.
16. **Brown RS, Demmer LA.** The etiology of thyroid dysgenesis-still an enigma after all these years. *J Clin Endocrinol Metab*. 2002;87:4069–4071.
17. **Szinnai G.** Clinical genetics of congenital hypothyroidism. *Endocr Dev*. 2014;26:60–78.
18. **Cooper DS, Axelrod L, DeGroot LJ, Vickery AL Jr, Maloof F.** Congenital goiter and the development of metastatic follicular carcinoma with evidence for a leak of nonhormonal iodide: clinical, pathological, kinetic, and biochemical studies and a review of the literature. *J Clin Endocrinol Metab*. 1981;52:294–306.
19. **Camargo R, Limbert E, Gillam M, et al.** Aggressive metastatic follicular thyroid carcinoma with anaplastic transformation arising from a long-standing goiter in a patient with Pendred's syndrome. *Thyroid*. 2001;11:981–988.
20. **Alzahrani AS, Baitei EY, Zou M, Shi Y.** Clinical case seminar: metastatic follicular thyroid carcinoma arising from congenital goiter as a result of a novel splice donor site mutation in the thyroglobulin gene. *J Clin Endocrinol Metab*. 2006;91:740–746.
21. **Hishinuma A, Fukata S, Kakudo K, Murata Y, Ieiri T.** High incidence of thyroid cancer in long-standing goiters with thyroglobulin mutations. *Thyroid*. 2005;15:1079–1084.
22. **Medeiros-Neto G, Gil-Da-Costa MJ, Santos CL, et al.** Metastatic thyroid carcinoma arising from congenital goiter due to mutation in the thyroperoxidase gene. *J Clin Endocrinol Metab*. 1998;83:4162–4166.
23. **Yashiro T, Ito K, Akiba M, et al.** Papillary carcinoma of the thyroid arising from dyshormonogenetic goiter. *Endocrinol Jpn*. 1987;34:955–964.
24. **Raef H, Al-Rijjal R, Al-Shehri S, et al.** Biallelic p.R2223H mutation in the thyroglobulin gene causes thyroglobulin retention and severe hypothyroidism with subsequent development of thyroid carcinoma. *J Clin Endocrinol Metab*. 2010;95:1000–1006.
25. **Drut R, Moreno A.** Papillary carcinoma of the thyroid developed in congenital dyshormonogenetic hypothyroidism without goiter: diagnosis by FNAB. *Diagn Cytopathol*. 2009;37:707–709.

26. **Kallel R, Mnif Hachicha L, Mnif M, et al.** [Papillary carcinoma arising from dyshormonogenetic goiter]. *Ann Endocrinol (Paris)*. 2009;70:485–488.
27. **Muller PY, Janovjak H, Miserez AR, Dobbie Z.** Processing of gene expression data generated by quantitative real-time RT-PCR. *Biotechniques*. 2002;32:1372–1374, 1376, 1378–1379.
28. **Shibusawa N, Yamada M, Hirato J, Monden T, Satoh T, Mori M.** Requirement of thyrotropin-releasing hormone for the postnatal functions of pituitary thyrotrophs: ontogeny study of congenital tertiary hypothyroidism in mice. *Mol Endocrinol*. 2000;14:137–146.
29. **Milenkovic M, De Deken X, Jin L, et al.** Duox expression and related H2O2 measurement in mouse thyroid: onset in embryonic development and regulation by TSH in adult. *J Endocrinol*. 2007;192:615–626.
30. **Murakami M, Kamiya Y, Morimura T, et al.** Thyrotropin receptors in brown adipose tissue: thyrotropin stimulates type II iodothyronine deiodinase and uncoupling protein-1 in brown adipocytes. *Endocrinology*. 2001;142:1195–1201.